Experimental and theoretical analysis of friction stir welding of Al–Cu joints

Ahmed O. Al-Roubaiy, Saja M. Nabat & Andre D. L. Batako

The International Journal of Advanced Manufacturing Technology

ISSN 0268-3768

Int J Adv Manuf Technol
DOI 10.1007/s00170-013-5563-z

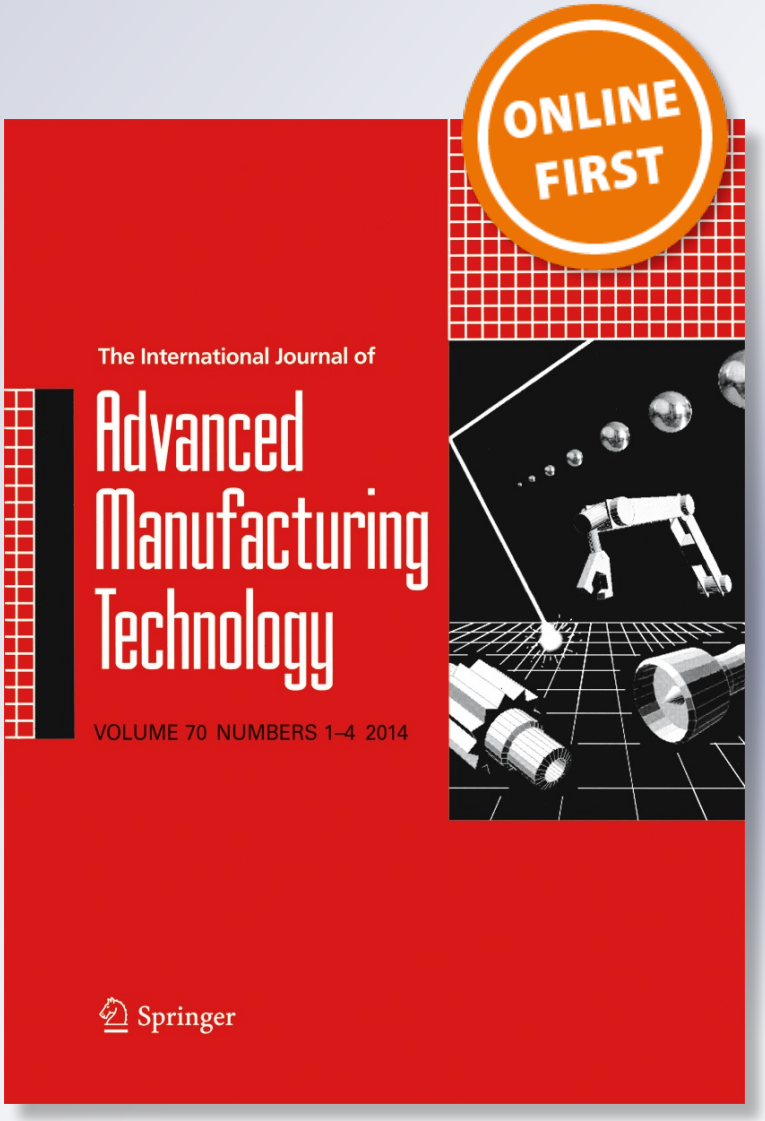

Springer

Int J Adv Manuf Technol
DOI 10.1007/s00170-013-5563-z

ORIGINAL ARTICLE

Experimental and theoretical analysis of friction stir welding of Al–Cu joints

Ahmed O. Al-Roubaiy · Saja M. Nabat · Andre D. L. Batako

Received: 5 June 2013 / Accepted: 16 December 2013

Abstract This paper presents a study of friction stir welding of aluminium and copper using experimental work and theoretical modelling. The 5083-H116 aluminium alloy and pure copper were successfully friction-stir-welded by offsetting the pin to the aluminium side and controlling the FSW parameters. A theoretical analysis is presented along with key findings. The process temperatures are predicted analytically using the inverse heat transfer method and correlated with experimental measurements. The temperature distribution in the immediate surroundings of the weld zone is investigated together with the microstructures and mechanical properties of the joint. This was supported by a finite element analysis using COMSOL Multiphysics. In this study, two rotational speeds were used and a range of offsets was applied to the pin. The microstructure analysis of the joints was undertaken. This revealed some particles of Cu inclusion in the nugget zone. The energy dispersive spectroscopy showed a higher diffusion rate of aluminium towards the interface while copper maintained a straight base line.

A. O. Al-Roubaiy
Materials Engineering Department, College of Engineering, Babylon University, Babylon, Iraq
e-mail: ahmed_rubai@yahoo.com

S. M. Nabat
Materials Engineering Department, College of Engineering, Kufa University, Kufa, Iraq
e-mail: ssaamhilla@yahoo.com

A. D. L. Batako (✉)
GERI, Liverpool John Moores University, Byrom Street, Liverpool L3 3AF, UK
e-mail: a.d.batako@ljmu.ac.uk

Published online: 17 January 2014

Keywords Friction stir welding · Aluminium · Copper · Dissimilar joint · Pin offset

1 Introduction

The joining of dissimilar materials is becoming increasingly important in industrial applications [1]. Many emerging applications such as power generation, chemical, petrochemical, nuclear, aerospace, transportation and electronic industries require the joining of dissimilar materials using different methods, especially friction welding and friction stir welding [2]. Due to the different chemical, mechanical and thermal properties of materials, the joining of dissimilar materials presents more challenges than joining similar materials.

Kimapong and Watanabe [3] carried out experiments in welding aluminium alloy 5083 to mild steel. They investigated the effects of pin rotation speed and the position of the pin axis on the tensile strength and microstructure of the joint. In their study, maximum tensile strength was obtained when the pin offset was 0.2 mm towards the steel. With large offset, the steel fragments scattering in the aluminium alloy matrix become larger in size leading to the formation of voids.

However, when joining dissimilar materials using friction stir welding (FSW), the problems arise not only from a material properties point of view but also from the possibility of the formation of brittle inter-metallic phases and low melting point eutectics. The inter-metallic compounds in an Al–Cu system were found in the friction welding of the oxygen-free copper to pure aluminium and in the cold roll welding of Al/Cu bimetal [2]. FSW has a greater potential of making high-quality welds with dissimilar material compared to fusion

welding. However, previous studies indicated that few sound dissimilar FSW joints were obtained.

Cu–Al joints are inevitable in certain applications due to unique performances such as higher electric and heat conductivity, corrosion resistance and mechanical properties. Consequently, Al and Cu are replacing steel in electricity supply systems due to their higher electric conductivity [4] in heat exchangers and various types of components in electrical machinery to obtain lightweight products [5]. One of the difficulties in Al–Cu joints is that the Al easily oxidizes at elevated temperature. Welding cracks are also observed in joints created by brazed or fusion of Al–Cu. Therefore, a high-quality weld joint of Al–Cu is difficult to obtain by means of conventional welding methods [6].

Li et al. [7] studied the microstructure and mechanical properties of the weld joint where pure copper was welded to 1350 aluminium alloy by FSW. They observed that the hardness in the copper side was higher than the aluminium side. They also showed that there were no inter-metallic formations in the interface between the copper and aluminium. Their work revealed a mixed ductile fracture during tensile tests of the joints.

Galvao et al. [8] investigated the influence of the FSW process parameters on the formation and distribution of inter-metallic phases at the interface of the joint between the copper and aluminium. Their work pointed out that under lower heat input, only a thin inter-metallic layer distribution along Al/Cu interface was formed inside the nugget. They reported that increasing the heat input promoted material mixing and the formation of increasing amount of a rich inter-metallic structure.

Lui et al. [9] used a butt barrier method to achieve a better appearance of the weld. Their work showed that the voids in the weld decreased with the increase of the pin rotational speed (1,000 rpm). However, this improvement reached a critical speed (1,500 rpm) where the voids began to increase.

Xue et al. [10] investigated the effect of welding parameters on mechanical properties, the interface microstructure and surface morphology for butt joining of 1060 aluminium alloy and pure copper. They obtained a good defect-free joint only when the hard Cu plate was fixed at the advancing side. A large volume defect was observed when the soft Al plate was placed at the advancing side. Their experiments also obtained good defect-free joints under large pin offsets of no less than 2 mm to the Al matrix. A good metallurgical bonding between the Cu bulk/pieces and Al matrix was achieved.

Bisadi et al. [11] studied FSW for joining sheets of AA5083 aluminium alloy with pure copper and the effects of process parameters including rotational and welding speeds on the microstructures and mechanical properties of the different joints. The experiments were performed at rotational speeds of 600, 825, 1,115 and 1,550 rpm. Two welding speeds of 15 and 32 mm/min were applied for each case. It was observed that very low or very high welding temperatures led to joint defects. In their work, the inter-metallic compounds and their effects on the mechanical properties of the joints were investigated. The best joint tensile shear properties were achieved at the rotational speed of 825 rpm and welding speed of 32 mm/min.

Galvão et al. [12] analysed and compared the influence of the welding conditions on the evolution of the torque during similar and dissimilar friction stir butt welding of 5083-H111 aluminium alloy and copper. They observed that the average torque is strongly affected by the materials to be welded, since, for all welding parameters, the lowest average torque values were registered during dissimilar welding. Some differences in instantaneous torque evolution, during welding, were observed depending on base material combinations. A strong fluctuation in instantaneous torque was registered in dissimilar welding with the copper at the advancing side. This was related with the large inter-metallic content in the welds.

Genevois et al. [13] investigated the joining of A1050 aluminium alloy with commercially pure copper by friction stir welding. The pin tool was located exclusively on the Al side, and there was no mixing of either material through the weld. The bonding resulted only from the reactive inter-diffusion; therefore, this process is named friction stir diffusion bonding. The reactive inter-diffusion of Al and Cu led to the formation of a very thin layer (200 nm) of inter-metallic compounds at the Al/Cu interface. The analysis of the microstructure indicated that this thin layer was formed after the stirring action of the tool pin. Two inter-metallic compounds were detected, namely the Al_2Cu (θ) and Al_4Cu_9 (γ) phases.

Lambrakos et al. [14] used an inverse problem approach to the analysis of friction stir welding where they used thermocouple measurements as input information. The calculated temperature field is scaled according to the peak temperature measured by a thermocouple at a specific point on the bottom surface of the workpiece.

In this paper, high-quality Al–Cu joints were successfully achieved by offsetting the pin to the Al side and controlling the FSW parameters. The microstructures and mechanical properties of the obtained joints were investigated. The purpose of this work is to study the capability of joining Al–Cu and the effect of FSW parameters on the quality of the joint. The distribution of the temperatures and the heat flux during this process is also investigated.

2 Experimental procedures

Aluminium alloy (5086-H116) and pure copper (99.972 % purity) plates were butt-welded using an AJAX universal milling machine. The dimensions of the plates were 200× 100×6.3 mm. In this experiment, key locations of the thermocouples were defined, and holes of 1.5 mm in diameter and

3 mm were drilled in the plate surface to accommodate thermocouple wires.

Chromel and Alumel thermocouple wires of type (K) were obtained from Omega Eng. Inc. Using these wires, thermocouple tips (0.25 mm diameter) were welded in-house using a laboratory instrument welder. The thermocouples were fixed in the holes using copper fibres; therefore, the thermocouples were securely embedded in the holes, and the temperatures were measured directly without any external disturbances. Figure 1 illustrates the configuration of the thermocouples imbedded in the two plates to be welded. The temperatures were recorded in real time using a data logging system with 12 channels linked to the thermocouples.

In this study, the thermocouples were installed at equal distance on both sides of the axis of the pin linear displacement. Consequently, the thermocouple in ch7 is located at 13 mm away from the centre line of the pin into the aluminium side, whilst the thermocouple in ch2 is displaced 13 mm away from the centre line of the pin into the copper side. This provides a 26-mm space between the thermocouples as illustrated in Fig. 1.

The Al plate was positioned in the retreating side, while the copper plate was in the advancing side as illustrated in Fig. 2a. The Al and Cu plates were prepared in order to remove the oxide layer using an abrasive process, then cleaned with acetone. The welding process progressed as follows: The welding starts by plunging a rotating pin into the soft material (Al) to avoid pin erosion or breaking. The rotating pin is then pushed towards the faying surface of the copper with a specific pin offset. The pin offset is the distance from the side of pin to the butt line; this is denoted by the sign (−) in Al and (+) in Cu, and (0) indicates when the pin side is just touching the butt line (Cu) as shown in Fig. 2.

In this experiment, the pin offset was set in the range of 0 to 0.4 mm; the rotational speed was set to 560 and 710 rpm with constant: welding speed of 69 mm/min. The tilt angle was 2° and a plunging depth of 0.25 mm was applied with a dwelling time of 20 s. A cylindrical tool with a counter threaded pin and

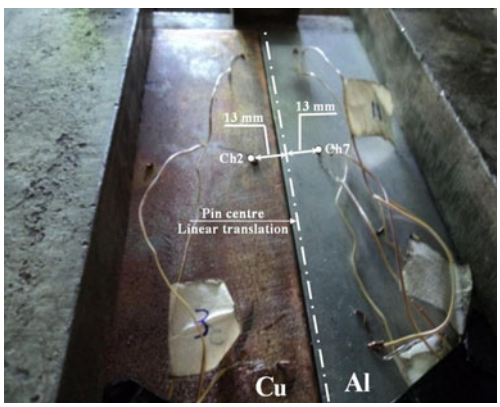

Fig. 1 The thermocouple implementation

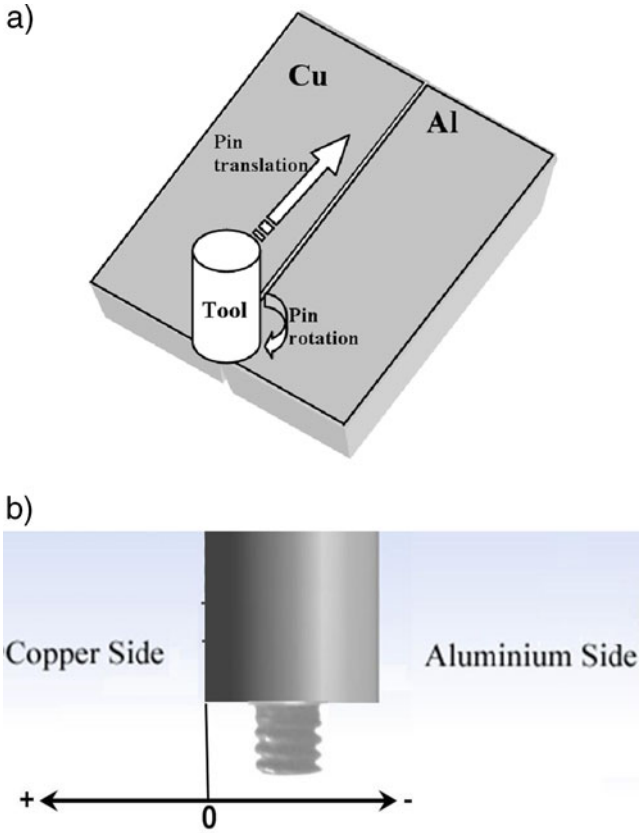

Fig. 2 Schematic of system configuration: **a** pin position relative to plates; **b** coordinate system and pin offset

concaved shoulder was used, while the angle between the edge of shoulder and the pin was 10°. The shoulder was 18 mm in diameter and the pin diameter was 6 mm with a height of 5.9 mm which slightly less than material thickness (6.3 mm). The tool was made of chromium alloy steel.

The results of the welding experiments are illustrated in Fig. 3, where dog-bone samples were prepared for uniaxial tensile tests. Tensile specimens were machined according to the ASTM B 557M-02 standard. Microhardness tests were carried out using a Digital Microhardness tester, type HV-1000) TH-717.

A detailed examination of the joints was undertaken at the normal cross section (plane normal to welding direction) and at the longitudinal cross section (plane parallel to welding direction). An optical microscopy system was used in this study.

3 Modelling of the FSW process

In general, problems governed by differential equations can be solved by approximating the problem with a numerical method. In this study, the numerical method used was based on the approach reported by Nandan et al. [15]. A numerical modelling is the division of a geometrical domain into a finite

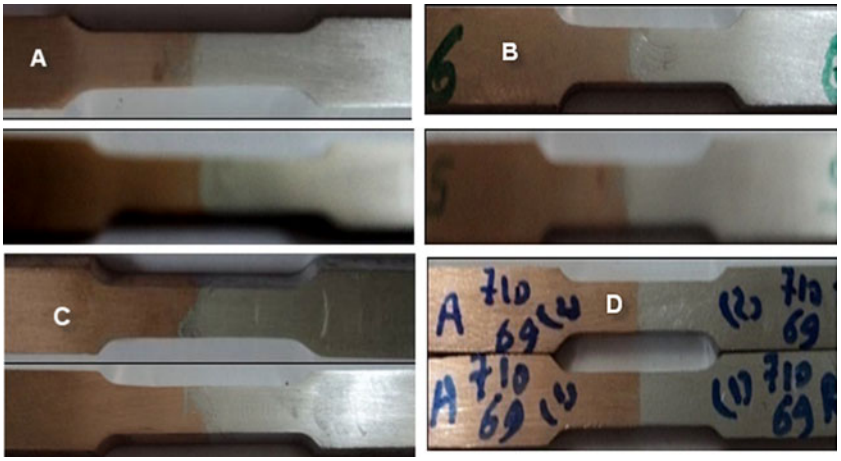

Fig. 3 Tensile test specimens for Al–Cu welded at **a** 560 rpm and 0.2 mm offset, **b** 560 rpm and 0.3 mm offset, **c** 710 rpm and 0.2 mm offset and **d** 710 rpm and 0.3 mm offset

number of nodal points and elemental volumes. In addition, an approximation of the governing boundary conditions affecting each nodal point and its neighbouring points is defined. Solutions are sought for the system of equations resulting from this approximation.

3.1 Heat generated at the tool shoulder/workpiece interface

During FSW, heat is generated by friction between the tool and the work piece as well as the plastic deformation of materials. The dominating heat generation mechanism is influenced by the weld parameters, thermal conductivities of the workpiece, pin tool and backing anvil [15]. Early experimental studies showed that the majority of the heat generation occurs at the shoulder/workpiece interface. The controlling mechanism of heating is due to either friction or plastic dissipation, depending on the contact conditions between the two surfaces. The weld tool geometric features of both the pin and the shoulder influence whether the two surfaces slide, stick or alternate between the two modes. More recent analytical studies have indicated that the heat generated between the pin tool and the workpiece is not insignificant and should be included in defining the heat field. The amount of heat input from deformational heating around the pin has been estimated to range from 2 [16] to 20 % [17]. The local friction force at every point can be calculated as [18, 19]:

$$F_{\mathrm{f}} = \mu F_{\mathrm{n}} \tag{1}$$

where F_{f} is the frictional force (N), F_{n} is the normal force applied to the workpiece (N) and μ is the coefficient of friction. Therefore, heat generation rate is expressed as:

$$q = v F_{\mathrm{f}} \tag{2}$$

where (q) is the heat generation rate (in Newton meters per second) and v is the relative slip velocity (in meters

Table 1 Thermal properties of the materials used in this study [20]

Properties	Copper		Aluminium	
	20 °C	500 °C	20 °C	500 °C
Specific heat (Cal/g/°C)	0.09	0.11	0.21	0.26
Thermal conductivity (Cal/cm/s/°C)	0.94	0.85	0.53	0.4
Coefficient of linear thermal expansion ($\alpha \times 10^{-6}$)	16	20	23	30

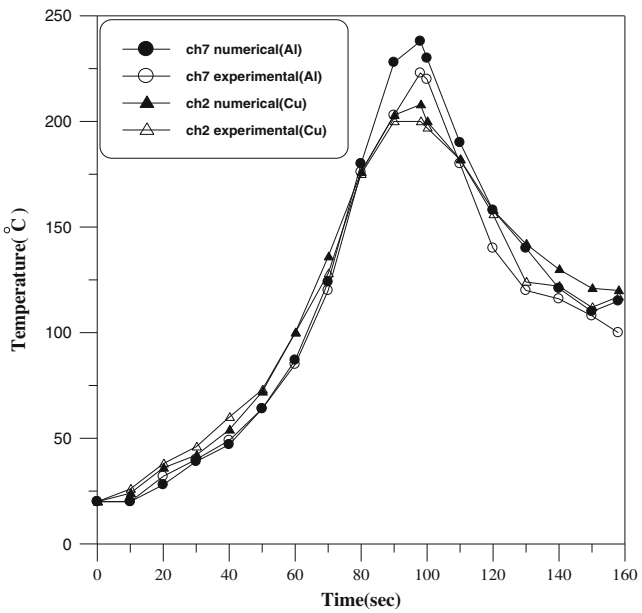

Fig. 4 Temperature distribution in Al and Cu sides at ch2

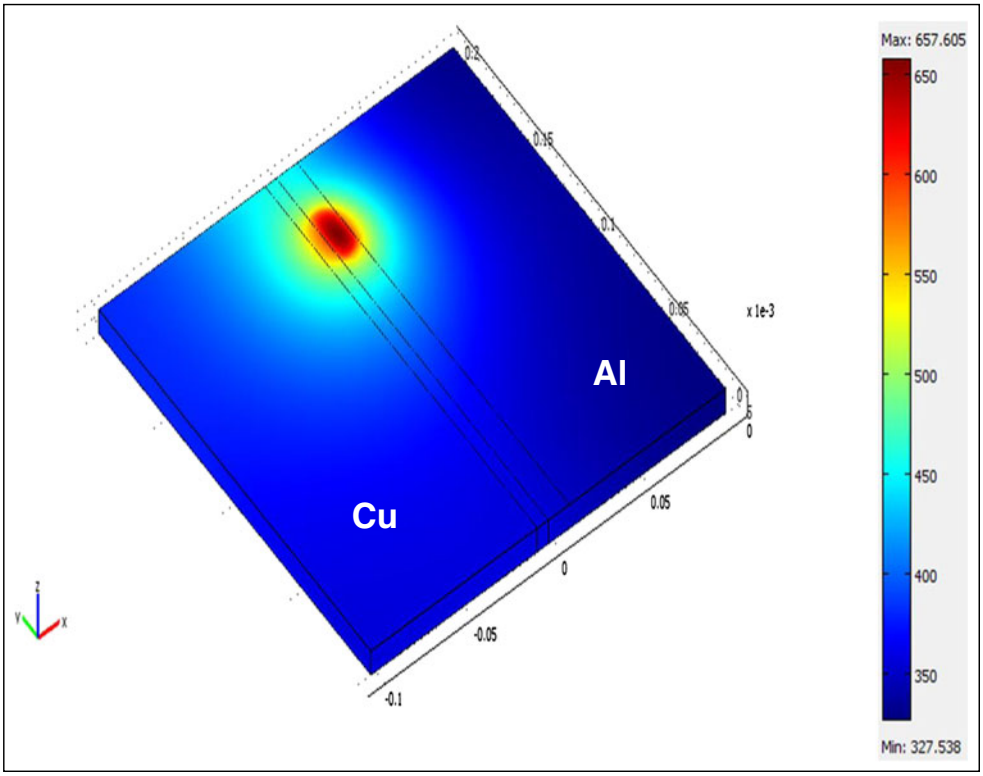

Fig. 5 Temperature contours in kelvin at (710 rpm and 69 mm/min)

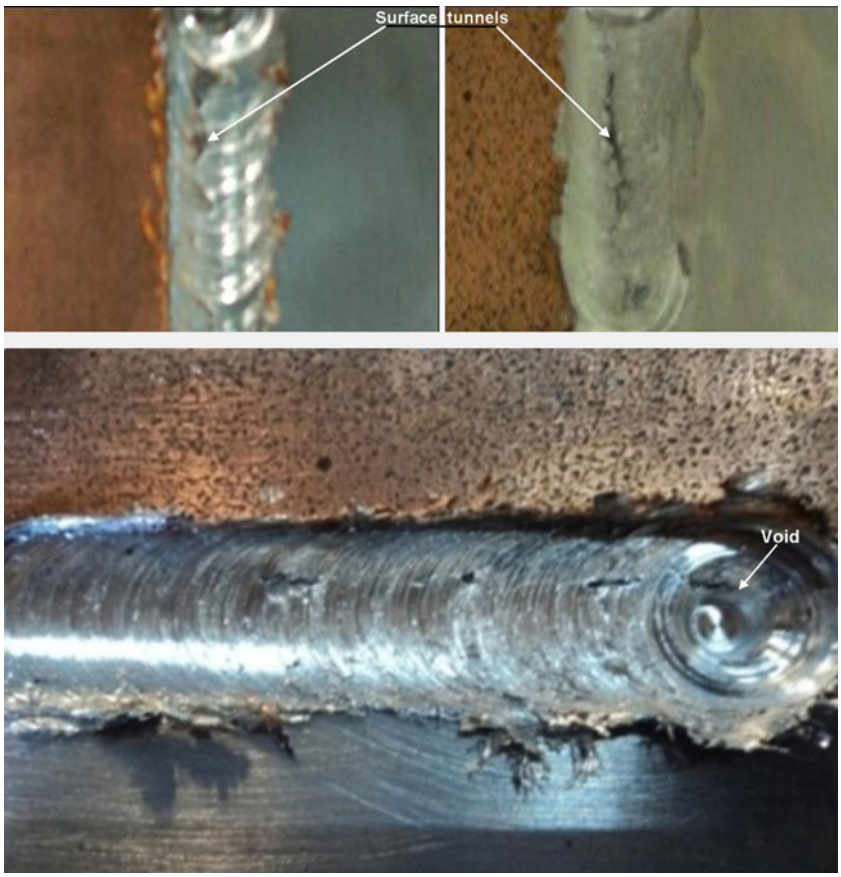

Fig. 6 Surface tunnel and void formation

Fig. 7 Internal tunnel

per second), which is then defined as $v=R\omega$ and $\omega=2\pi\ n$; therefore,

$$q = 2\pi\mu nRF_{\mathrm{n}} \tag{3}$$

where R is the distance from the calculated point to the axis of the tool rotation and n is the rotational speed of the tool (in revolutions per second). Also q can be estimated when the spindle torque (T) is known as in Eq. (4) below.

$$q = T\omega \tag{4}$$

3.2 Thermal model

A thermal model was used to calculate the transient temperature fields developed in the workpiece during friction stir welding. The model is based on 3D geometry with Lagrange—T_2 J_1 element. The total numbers of tetrahedral and boundary elements (triangular) were 9,081 and 4,192, respectively.

In the thermal analysis, the transient temperature field T which is a function of time t and the spatial coordinates (x, y) is estimated by the 3D nonlinear heat transfer equation [19]:

$$k\left(\frac{\partial^2 T}{\partial^2 x^2}+\frac{\partial^2 T}{\partial^2 y^2}+\frac{\partial^2 T}{\partial^2 z^2}\right)+Q_{\mathrm{int}}=C_{\mathrm{p}}\rho\frac{\partial T}{\partial t} \tag{5}$$

where k is the coefficient of thermal conductivity, Q_{int} is the internal heat source rate, C_{p} is the mass specific heat capacity and ρ is the density of the materials.

In this study, the following assumptions were made. The radiation heat flux was considered to be negligible. The heat transfer from the workpiece to the tool was also neglected. It was assumed that no melting occurred during the welding process, and the workpiece material was considered isotropic and homogeneous. Both materials were rigidly attached along the interface, and the effect of friction between attached materials was taken into consideration; therefore, friction coefficient was ignored. The dependence of thermal properties of materials on temperature was adopted from Roth [20] (see Table 1).

The software package "COMSOL Multiphysics" was used to specify the boundary conditions for FSW thermal model. The convective heat loss occurs across all the free surface of the workpiece, and the convective heat loss (q_{s}) into the ambient was estimated as follows [19]:

$$q_{\mathrm{s}} = -k\left.\frac{\partial T}{\partial n}\right|_{\text{free-surface}} = h_{\infty}(T-T_{\infty}) \tag{6}$$

where k is the coefficient of thermal conductivity of the work piece, n is the direction coordinate, h_{∞} is the ambient convection coefficient (typically taken as 10 W/m^2 K) for an ambient temperature of 293 K and T_{∞} is the ambient temperature (in kelvin).

In order to account for the conductive heat loss from welded plates to backing plate, a high overall heat transfer coefficient was assumed. This assumption is based on the previous studies [19, 21–23]. The heat loss was approximated by a fictitious convection heat flux loss (q_{f}) given in the Eq. (7):

$$q_{\mathrm{f}} = h_{\mathrm{f}}(T-T_{\infty}) \tag{7}$$

where h_{f} is a fictitious convection coefficient which is a simplified convective coefficient at the contact surfaces between the weld plates and the backing plate due to the complexity involved in obtaining the exact contact condition between these surfaces. The value of h_{f} was guesstimated using an inverse analysis method.

3.3 Inverse analysis method for heat transfer

In order to estimate the heat flux generated in the process using Eqs. (3) and (4), the normal force applied to the workpiece or spindle torque must be known. Conversely, to estimate q_{f} in Eq. (7), h_{f} must be known. Therefore to overcome

Table 2 Tensile test results of Al-Cu joint welded at 69 mm/min

Sample number	Tool rotating speed (rpm)	Pin offset (mm)	Tensile strength (MPa)
A	560	0.2	199.8
B	560	0.3	191
C	710	0.2	206.7
D	710	0.3	198.21

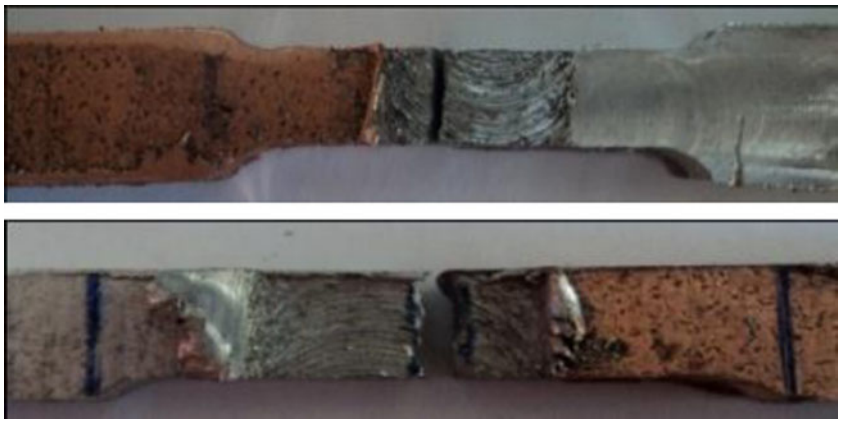

Fig. 8 Tensile test sample failure during machining

these problems, a commercial finite element analysis package (COMSOL) was used to predict the heat flux q_f and h_f in an inverse analysis method. The inverse analysis method operated on the basis of seven steps was described as follows:

1. In COMSOL, specify a "guess" value for the heat flux (at constant h_f) in the friction zone between the tool and the plates which was initially set at 10^6(W/m^2).
2. Specify a "guess" value for the fictitious convection coefficient (h_f) in the equation which was initially set to 20 times of the convention coefficient of the air.
3. Run the prediction model and observe its output by continuously comparing it to the measured temperature at specific location on the plates. Once an agreement between the two values is reached, the heat flux and h_f are then output as sought values.
4. Solve numerically Eq. (5) with the specified boundary conditions.
5. Compare the variations of temperature in time obtained from the prediction model and from the experimental measurement at the specific locations.
6. Adjust the values of the heat flux and h_f based on the differences of temperature determined in step 4.
7. Repeat the steps (1)–(6) until the numerical temperature distributions are in good agreement with the experimental data at all points of observation.

The magnitude of the heat flux controls the peak value of the temperature distribution curve, while the value of h_f controls the shape of the temperature distribution curve.

4 Results and discussion

4.1 Results of the inverse analysis method for heat transfer

One of the very important parameters in measuring the heat distribution during joining is the estimation of the heat flux between shoulder and workpiece; this was found by an inverse analysis method. During the experimental work, the actual process power of the milling machine operating at 710 rpm, 69 mm/min was unknown. However, knowing the cross-sectional area of shoulder and the pin offset of 0.2 mm, the heat flux required for joining Al–Cu was estimated using the inverse method, which provided a value of 2.36×10^6 W/m^2. Applying this method, the unknown convection coefficient h_f between the weld plates and the backing plate estimated as 230 W/m^2 K.

4.2 Temperatures distribution

During the FSW experiment, the transient temperature distributions were recorded with K-type thermocouple, and a numerical temperature distribution was predicted with the commercial finite element analysis program COMSOL. The welding parameters for Al–Cu joint were 710 rpm, 69 mm/min and 0.2 mm pin offset. The temperatures were recorded at 3 mm which was the middle of the plate of 6 mm in thickness. Due the difficulties encountered in locating a thermocouple at the interface between the two weld plates, which could be damaged by the moving shoulder, the measurement was taken at 13 mm from the interface. For the Al–Cu joint shown in Fig. 4, there are clear differences in the temperature distribution between the aluminium (retreating side) and the copper (advancing side) due the differences in thermal properties, especially the thermal conductivity (k) between the two

Fig. 9 Tensile test specimen after fracture for Al–Cu joint

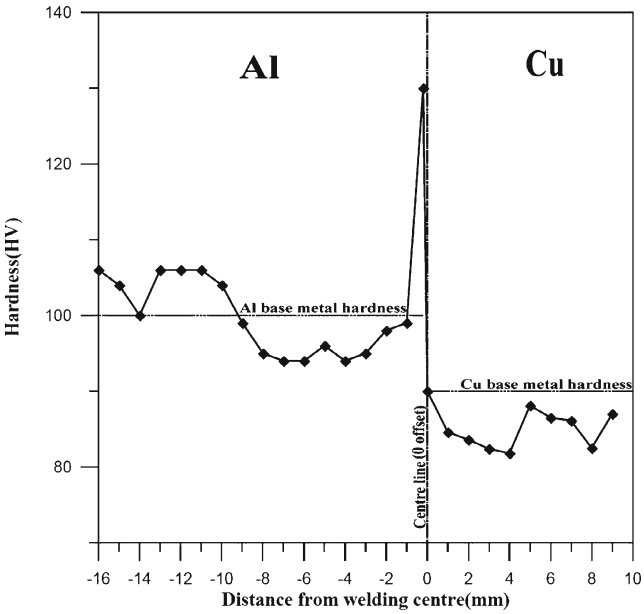

Fig. 10 Microhardness profile for Al–Cu joint at (710 rpm and 0.2 mm pin offset)

materials, where *k* for copper about three times the conductivity of 5083-H116 aluminium alloy. Here the peak temperature for the Al is higher than for the Cu (about 27 °C numerically and 23 °C experimentally). Also different rates of heating and cooling between the two sides were observed where a higher rate of heating and cooling was noticed in the Cu than the Al due to the higher thermal conductivity of Cu. The temperature distribution in the Al–Cu joint showed that there is a convergence between numerical and experimental results.

4.3 Temperature contours

One of the advantages of FEM analysis is the provision of temperature contours in joined plates, which gives a full idea of temperature at any point in the joint. One example of a contour plot for the Al–Cu joint is shown in Fig. 5, where a significant difference in temperature distribution between the Al and Cu sides is observed. Here there is high heat dissipation in the Cu side due to the difference in thermal properties of Cu and Al (especially thermal conductivity). In Fig. 5, the maximum temperature in the simulation is 657 Kat the centre line of the weld line. However, the maximum temperature measured during the experimental at the point ch7 is about 240 °C (≈513 K). This is because in the experimental measurements of the thermocouples were located at 13 mm away from the centre line to avoid cutting through the thermocouple.

4.4 Weld defects

The defects shown in Fig. 6 are termed "surface tunnel" and voids which are due to insufficient plunging depth. A small plunging depth caused by a light axial force leads to an insufficient refilling of the advancing side of the nugget. Therefore, the appearance of surface tunnels can be minimized by increasing the axial force of the FSW tool through an increased plunging depth. By increasing the force, the forging pressure inside the weld nugget may also collapse the voids and promote the convergence of the material.

These defects also appear when the offset in the Al side is too large (equal or greater than 0.4 mm). This is because the Cu fragments became larger or when there is a gap between two weld workpieces. Some defects were also observed in the joints with 0.4 mm offset with subsequent lowered joint strength.

Surface tunnel and voids are generally found on the advancing side of the weld, and they may or may not break through to the surface of the friction stir weld. For a given tool design, void formations are due to insufficient forging pressure, too high of welding speed and insufficient workpiece clamping(too large of joint gap). Design of the pin and shoulders may play role to information of these defects. FSW parameters also affected to create these defects by lack of heat and the deformed materials cool before the material can fully fill the region directly behind the tool. Insufficient cleaning and imperfections on the faying surfaces before cause these defects.

"Internal tunnels" are voids or channels in the weld body (cross section) as illustrated in Fig. 7. These are generated when the pin is too long and/or the pin diameter is too large. This defect also appears when a large offset is applied to the pin.

4.5 Tensile test results

Table 2 shows the results of tensile tests for the Al–Cu joints with different welding parameters. When a zero or negative pin offset is applied, the specimens failed due to cracks during the preparatory machining. A sample of failed dog-bone specimens is shown in Fig. 8. This was caused by a poor or near absence of stirring action in the Cu side, which led to the shifting of the weld nugget into the Al side. Observation of the broken samples shows that there is no Cu content in the nugget zone.

Fig. 11 Photograph of normal cross section of Al–Cu joint

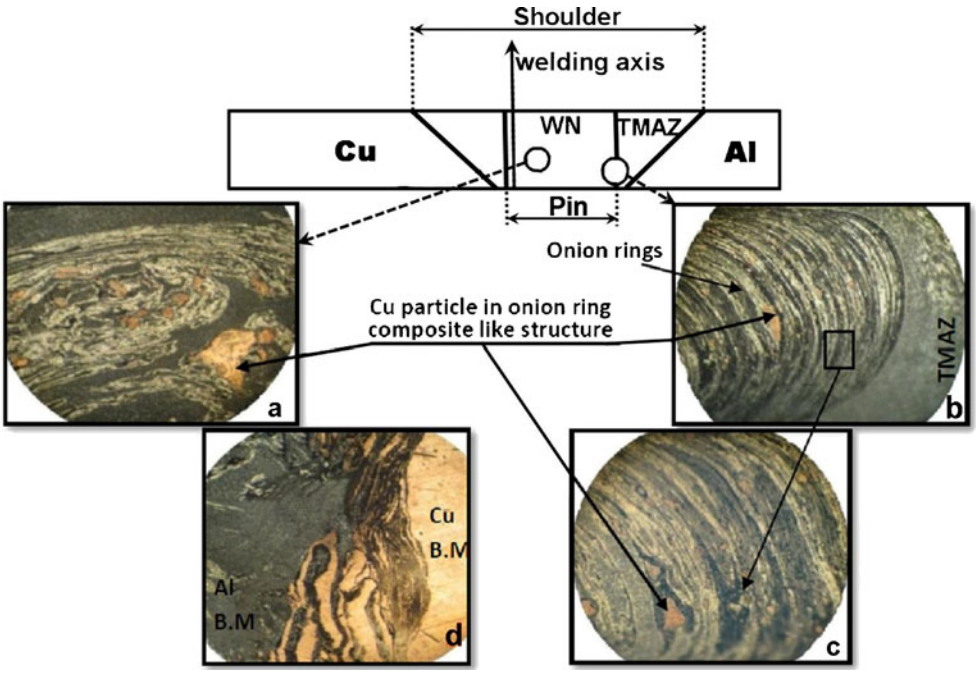

Fig. 12 Micrographs for Al–Cu joint showing *a* and *b* onion ring in WN at ×100, *c* onion ring at ×200 and *d* the interface between Al–Cu at ×100

The maximum tensile strength of the Al–Cu joint was 206.7 MPa at 710 rpm with 0.2 mm pin offset. This is due to the strengthening effect of Cu particles in the nugget zone and solid solution strengthening. As illustrated in Fig. 9, the fracture of the specimens occurred in the weld nugget at the Al side as shown. With the increase of the pin offset, the amount and size of Cu particles increased until the pin offset reached 0.4 mm, where defect formation began.

4.6 Hardness test

The microhardness profile of the Al–Cu joint is shown in Fig. 10, where the maximum hardness was observed at the interface. In the weld nugget, there was a mixture of randomly sized Cu particles, and the more this mixture of the particles, the more it led to a composite like reinforced aluminium matrix. Consequently, this composite structure had an inherent higher hardness. However, moving away from the interface towards the Al, a decrease of the hardness is observed in the graph. This is explained by the coarse grains in the heat-affected zone (HAZ). This decreased in hardness of the HAZ is due to the fact that both materials purchased in cold work processed condition and subsequent welding with high temperatures led to a recovery process in the materials. Thus, in the deformed zone of the structure, a re-crystallization and grain growth occurred depending on temperatures. This could have led to the formation of new strain-free grains and subsequently lowered the hardness of the deformed zone compared

Fig. 13 Micrograph longitudinal cross sections in weld nugget at ×100

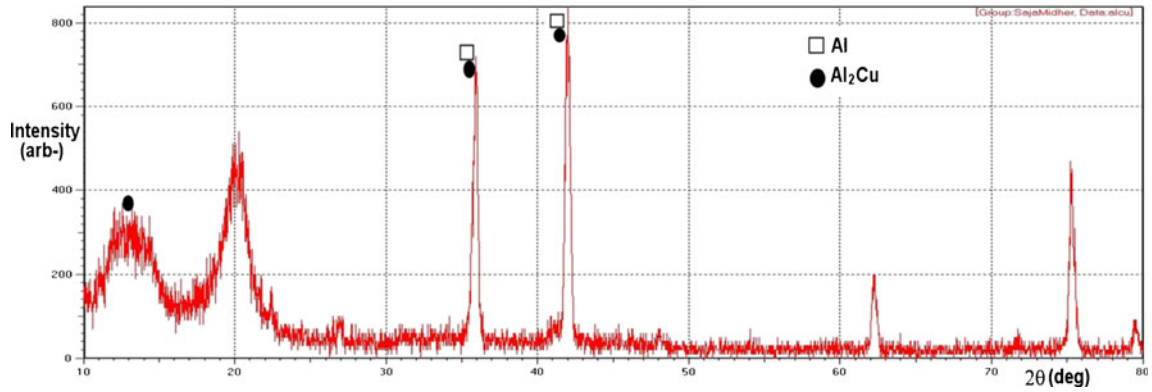

Fig. 14 X-ray diffraction pattern of the cross section of Al–Cu joint

to the base metal. It is possible that during the microhardness tests, the reading was taken at large or strain free grains.

4.7 Microstructure examination

A microstructure examination of Al–Cu butt joint at rotational speeds of 560 and 710 rpm with a welding speed of 69 mm/min and pin offset (0.2 mm) was conducted. The details of joint normal cross section (plane normal to welding direction) and longitudinal cross section (plane parallel to welding direction) were examined with optical microscopy. Two types of samples were used, i.e. with and without etching.

The normal cross section of Al–Cu joint without etching is shown in Fig. 11, where there are no defects or voids in the joint. After etching as shown in Fig. 12, it is observed that particles of Cu detached from the bulk of Cu metal created a dispersion strengthening in the Al matrix. Figure 14 supports that there are some intermetallic hard compounds of Al_2Cu imbedded in the ductile matrix of Al. The onion-ring shape in the weld nugget was achieved, which contains many particles of copper as shown in Fig. 12 a–c. The weld nugget can be considered as the aluminium matrix composite. The particles in the aluminium matrix of the nugget zone are attributed to the stirring action of the threaded pin that scraped Cu particles from the bulk copper, breaking up and dispersing them during

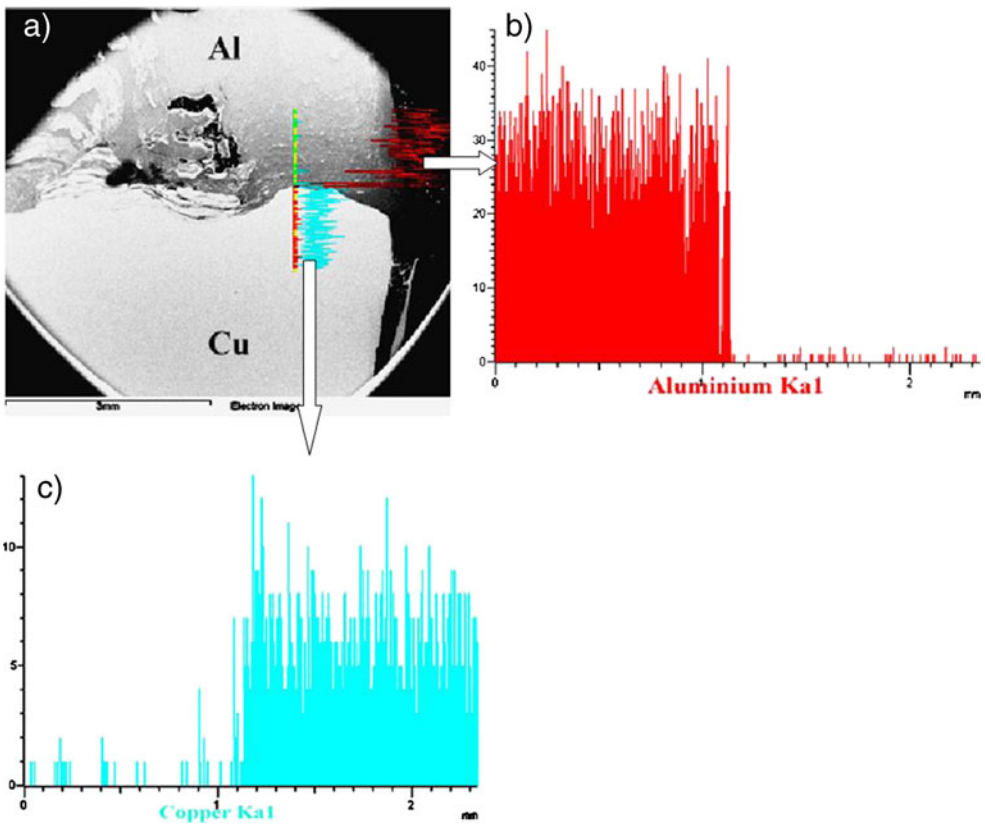

Fig. 15 SEM with EDS analysis of Al–Cu joint cross section: *a* diffusion of elements at joint boundary; *b* diffusion intensity of aluminium along scan line; *c* diffusion intensity of copper along scan line

the FSW process. The Cu particles were transported from the advancing side and deposited in the Al side (retreating side). The interface between the two metals showed a non-linear or irregular shape, which means that the welding pin stirred the butted surface of the copper side as shown in Fig. 12 d, where WN is the weld nugget, TMAZ is the thermomechanical affected zone and BM is the base metal.

Figure 13 illustrates the longitudinal cross section of the weld nugget where many fragments of copper are observed. The X-ray diffraction (XRD) analysis of the weld nugget detected an Al_2Cu intermetallic phase which supports the strengthening of this zone. This intermetallic compound was found in the interface as continuous non-linear shaped layer and in the weld nugget zone on the Al side as dispersed particles which give reinforcing effect in this zone. However, the intermetallic inclusions have a double effect, i.e. strengthening in very thin layers but lead to brittle behaviour in thick layer, e.g. cracks.

From XRD analysis (Fig. 14), the weld nugget contains Al_2Cu intermetallic compounds which give reasons for the strength of this zone; these intermetallic compounds were found in the interface as continuous non-linear shape layer and in the weld nugget zone in the Al side as dispersed particles which give a reinforcing effect in this zone.

Figure 15 is the SEM backscattered electron image at the interface between the Al–Cu joint. The cross section of the joint is illustrated in Fig. 15, whereas the surface of the joint is depicted in Fig. 16. Discontinuous reaction layers are observed in the interface where some fragments of Cu were pushed towards aluminium.

The energy dispersive spectroscopy (EDS) analysis showed the higher diffusion rate of aluminium element towards interface while the copper was pushed almost in a straight line into the Al base. Magnesium as a major element in Al alloy also was pushed into the copper base as scattered spots. This difference in diffusion behaviours between aluminium, copper and magnesium may be due to the fact that the diffusion rate of the aluminium element is greater than copper and magnesium. Some voids and cracks are observed near the interface and in the copper base side. This occurred due to brittle intermetallic compounds created at high friction temperature during welding process.

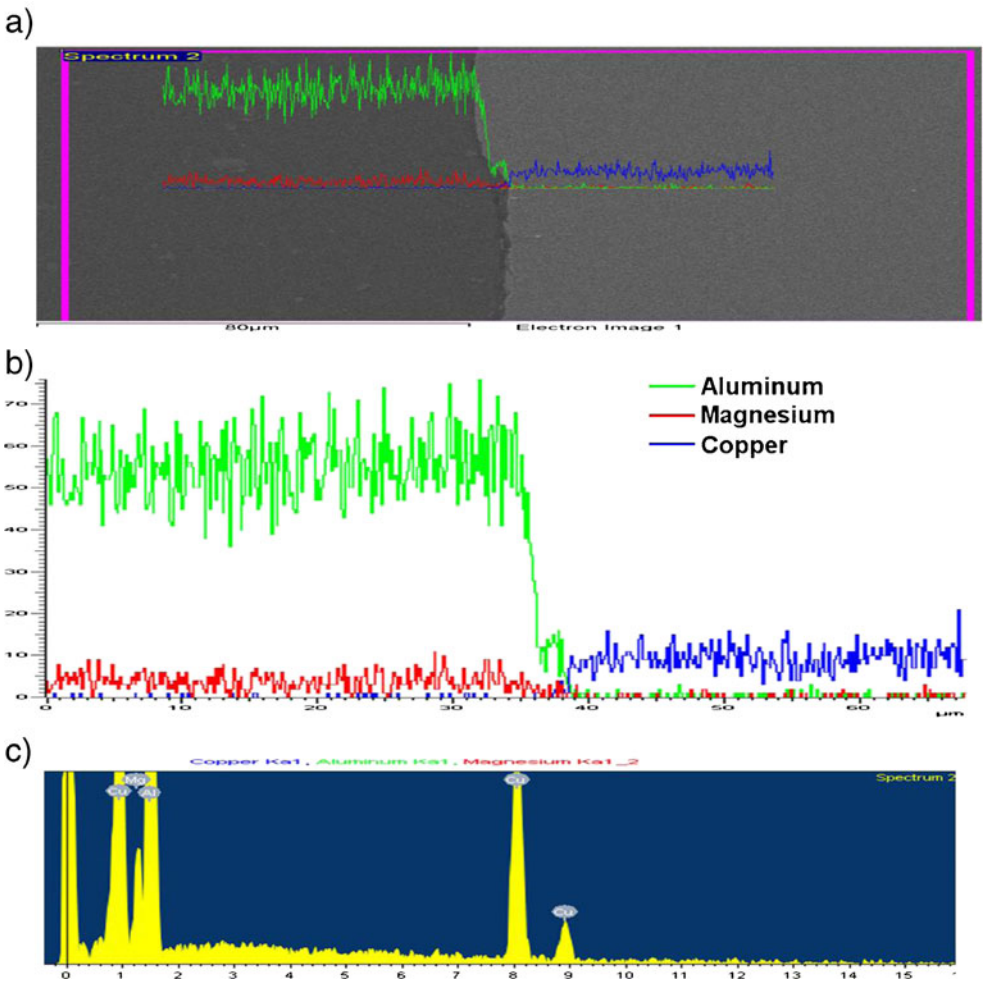

Fig. 16 SEM with EDS analysis of the joint top surface: **a** analysis line scan of diffusion of elements across the interface; **b** spectrum analysis of element diffusion across the joint interface; **c** element content and distribution in the scanned area

5 Conclusions

In this study, sound FSW Al–Cu joints were successfully achieved by friction stir welding technology. A thermal model was presented to predict the temperatures during the FSW process.

1. It was identified that it is practically difficult (almost impossible) to obtain a high-quality Al–Cu direct joint without offsetting the pin in the softer material (aluminium).
2. The experimental work revealed that the maximum tensile strength for Al–Cu joint was 206.7 MPa, which was obtained at a rotation speed of 710 rpm, welding speed of 69 mm/min and 0.2 mm pin offset.
3. The Al–Cu joint contained many Cu particles of inhomogeneous shape and distribution which were dispersed in the nugget zone; therefore, the weld nugget was reinforced by the included Cu particles. Some voids and cracks were observed in aluminium side.
4. It was identified experimentally and theoretically that the heat dissipation in the Cu side was higher than in the Al alloy side. This was supported by a good agreement between the experiment and the modelling.
5. Observation of the SEM and EDS reveals a step drop in the diffusion rate of the Al across the interface. However, Cu and Mg had a little or no change in concentration through the interface.

References

1. Xue P, Xiao BL, Ni DR, Ma ZY (2010) Enhanced mechanical properties of friction stir welded dissimilar Al–Cu joint by intermetallic compounds. J Mater Sci Eng A 527:5723–5727
2. Ouyang J, Yarrapareddy E, Kovacevic R (2006) Microstructural evolution in the friction stir welded 6061 aluminum alloy (T6-temper condition) to copper. J Mater Process Technol 172:110–122
3. Kimapong K, Watanabe T (2004) Friction stir welding of aluminum alloy to steel. Weld J 83(10):277–282
4. Sahin M (2010) Joining of aluminium and copper materials with friction welding. Int J Adv Manuf Technol 49:527–534
5. Ochi H, Ogawa K, Yamamoto Y, Kawai G, Sawai T (2004) The formation of intermetallic compounds in aluminium alloy to copper friction-welded joints and their effect on joint efficiency. Weld Int 18(7):516–523
6. Liu P, Shi Q, Wang W, Wang X, Zhang Z (2008) Microstructure and XRD analysis of FSW joints for copper T2/aluminium 5A06 dissimilar materials. J Mater Lett 62:4106–4108
7. Li X-W, Zhang D-T, Qiu C, Zhang W (2012) Microstructure and mechanical properties of dissimilar pure copper/1350 aluminium alloy butt joints by friction stir welding. Trans Nonferrous Met Soc China 22:1298–1306
8. Galvao I, Oliveira JC, Loureiro A, Rodrigues DM (2011) Formation and distribution of brittle structures in friction stir welding of aluminium and copper: influence of process parameters. Sci Technol Weld Join 16(8):681–689
9. Lui HJ, Shen JJ, Xie S, Huang YX, Cui F, Kuang LY (2012) Weld appearance and microstructural characteristics of friction stir butt barrier welded joints of aluminium alloy to copper. Sci Technol Weld Join 17–2:104–110
10. Xue P, Ni DR, Wang D, Xiao BL, Ma ZY (2011) Effect of friction stir welding parameters on the microstructure and mechanical properties of the dissimilar Al–Cu joints. Mater Sci Eng A 528 P:4683–4689
11. Bisadi H, Tavakoli A, Tour Sangsaraki M, Tour Sangsaraki K (2013) The influences of rotational and welding speeds on microstructures and mechanical properties of friction stir welded Al5083 and commercially pure copper sheets lap joints. Mater Des 43 P:80–88
12. Galvão, Leitão C, Loureiro A, Rodrigues DM (2012) Study of the welding conditions during similar and dissimilar aluminium and copper welding based on torque sensitivity analysis. Mater Des 42 P:259–264
13. Genevois C, Girard M, Huneau B, Sauvage X, Racineux G (2011) Interfacial reaction during friction stir welding of Al and Cu. Metall Mater Trans A 42–8:2290–2295
14. Lambrakos SG, Fonda RW, Milewski JO, Mitchell JE (2003) Analysis of friction stir welds using thermocouple measurements. J Sci Technol Weld Join 8(5):385–390
15. Nandan R, DebRoy T, Bhadeshia HKDH (2008) Recent advances in friction-stir welding—process, weldment structure and properties. J Prog Mater Sci 53(6):980–1023
16. Russell MJ, Shercliff HR (1999) Analytical modeling of microstructure development in friction stir welding. Proc. First Int. Symp. on Friction Stir Welding, Thousand Oaks, CA
17. Colegrove P, Painter M, Graham D, Miller T (2000) 3-dimensional flow and thermal modelling of the friction stir welding process. Second Int Symp On Friction Stir Welding (Gothenburg, Sweden)
18. Mohanad A (2007) Investigation of mechanical and microstructural characteristics of friction stir welded joints. Ph.D. thesis, Baghdad University, Iraq
19. Zhu XK, Chao YJ (2004) Numerical simulation of transient temperature and residual stresses in friction stir welding of 304L stainless steel. J Mater Process Technol 146(2):263–272
20. Roth A (1966) Vacuum sealing technology, 5th edn. Pergamon, New York
21. Mishra S, Mahoney MW (2007) Friction stir welding and processing. ASM International, Materials Park
22. Chao YJ, Qi X, Tang W (2003) Heat transfer in friction stir welding—experimental and numerical studies. J Manuf Sci Eng-Trans ASME 125(1):138–145
23. Rajesh N (2003) Friction stir welding: thermal effect of a parametric study on Buttan lap welds. M.Sc. thesis, India